Gold nanoparticles produce transient reactive gliosis in the adult brain

Article *in* Neuroscience Research · January 2021

DOI: 10.1016/j.neures.2020.12.003

CITATIONS
0

READS
97

5 authors, including:

Eduardo Lira
Universidad de Colima
2 PUBLICATIONS **5** CITATIONS
SEE PROFILE

María G. González- Pedroza
Universidad Autónoma del Estado de México (UAEM)
6 PUBLICATIONS **7** CITATIONS
SEE PROFILE

Raul Alberto Morales Luckie
Universidad Autónoma del Estado de México (UAEM)
60 PUBLICATIONS **762** CITATIONS
SEE PROFILE

Oscar Gonzalez-Perez
Universidad de Colima
102 PUBLICATIONS **4,065** CITATIONS
SEE PROFILE

Neuroscience Research xxx (xxxx) xxx–xxx

Contents lists available at ScienceDirect

Neuroscience Research

journal homepage: www.elsevier.com/locate/neures

Gold nanoparticles produce transient reactive gliosis in the adult brain

Eduardo Lira-Diaz[a,b], Maria G. Gonzalez-Pedroza[c], Clemente Vasquez[d], Raul A. Morales-Luckie[c], Oscar Gonzalez-Perez[a,*]

[a] Laboratory of Neuroscience, School of Psychology, University of Colima, Colima, 28040, Mexico
[b] Physiological Science PhD Program. School of Medicine, University of Colima, Colima, 28040, Mexico
[c] Department of Nanomaterials, Sustainable Chemistry Research Center, National Autonomous University of Mexico/Autonomous University of the State of Mexico, Toluca, 50200, Mexico
[d] University Center for Biomedical Research, University of Colima, Colima, 28040, Mexico

ARTICLE INFO

Article history:
Received 13 May 2020
Received in revised form 9 December 2020
Accepted 14 December 2020
Available online xxx

Keywords:
Nanoparticles
Astrocyte
GFAP
Microglia
Iba1
Astrogliosis

ABSTRACT

Gold nanoparticles (GNPs) have unique physical and chemical properties that allow them to function as a drug-delivery system for several tissues: skin, eye, liver, and others. However, information about the biological response of brain tissue against GNPs is limited. Astrocytes and microglia cells are the first line of defense against brain insults and proper indicators of the level of brain damage. This study was aimed to evaluate the astrocytic and microglia response after an intracerebral injection of polyethylene-glycol-coupled GNPs (PEGylated GNPs). We injected spherical PEGylated GNPs (85×10^6 nanoparticles /nl) with a glass micropipette (inner diameter =35 μm) into the striatum of P60 CD1 mice. We evaluated the cellular response of astrocytes and microglia on days 3, 7, 14, 30, and 90 after intracerebral injection. For both astrocytes and microglia cells, our findings indicated that the glial response was transient and mainly circumscribed to the injection site. This evidence suggests that PEGylated GNPs are well-tolerated by the neural tissue. Understanding the effects of GNPs in the adult brain is a crucial step to design proper pharmacological vehicles to deliver long-lasting drugs.

1. Introduction

Gold nanoparticles (GNPs) are solid structures of nanometric scale that can be produced with diverse shapes and sizes (1–100 nm) (ASTM, 2006; Shah et al., 2014). GNPs have a localized surface plasmon resonance (LSPR), surface functionalization and low toxicity, which are unique features that make them a safe tool for biological studies (Miao et al., 2018; Elahi et al., 2018). The chemical reactivity of GNPs allows them to interact with biologic molecules via covalent and non-covalent bonds (Austin et al., 2014). GNPs stability can be enhanced by coating their surface with polyethylene glycol (PEG), a polymer that prevents the uptake of gold nanoparticles by phagocytic cells and increases the nanoparticle half-life into the body (Amoozgar and Yeo, 2012; Sperling and Parak, 2010; Howard et al., 2008). These features make GNPs promising candidates for clinical applications (Shah et al., 2014; Austin et al., 2014). Malignant brain tumors (glioblastoma and high-grade astrocytoma), Alzheimer's disease, multiple sclerosis, Parkinson's disease, and other neurological disorders require long-acting formulations and a controlled release of drugs in specific brain regions. Hence, GNPs may be an appropriate vehicle for drug-delivery into the brain, but the effects of these nanoparticles in the neural tissue are not fully known.

Astrocytes and microglia cells are major neuroglial components of the CNS and the first cellular responders to brain damage (Sofroniew, 2009; Sofroniew and Vinters, 2010). Microglia cells are activated and guided by chemokines and cytokines released by a neural injury, where they phagocyte debris and present antigens (Nimmerjahn et al., 2005; Zamanian et al., 2012). Under pathological conditions, microglia cells suffer morphological changes, overexpress the ionized calcium-binding adapter molecule 1 (Iba1), and promote the activation of other neuroglial cells (Streit et al., 1988; Morioka et al., 1992). Brain injuries also activate astrocytes that overexpress the glial fibrillary acidic protein (GFAP). This activation process involves a gene rearrangement that produces morphological changes and proliferation (Sofroniew, 2009; Sofroniew and Vinters, 2010). Both microglia cells and astrocytes are cellular indicators of brain damage and may also indicate the magnitude of a neural injury (Burda and Sofroniew, 2014; Sofroniew, 2009). This study aimed to evaluate the astrocytic and microglia response after a GNPs administration at different time

* Corresponding author at: Facultad de Psicologia, Universidad de Colima, Av. Universidad 333, Colima, COL, 28040, Mexico.
E-mail address: osglez@ucol.mx (O. Gonzalez-Perez).

https://doi.org/10.1016/j.neures.2020.12.003
0168-0102/

points. We found that GNPs triggered cytoplasmic hypertrophy of astrocytes and microglia cells that is accompanied by an increase in the cell population. Microglia cell population returns to basal levels on the 14th-day post-injection, whereas the astrocyte population is normalized at 90 days post-injection. Our findings indicated that gold nanoparticles produced a transient and self-limiting reactive gliosis in the adult brain. Hence, this evidence suggests that gold nanoparticles may represent a safe tool for drug delivery into the brain parenchyma. This study is an initial approach that provides new clues for the design of studies that help design long-lasting drug carriers with clinical purposes.

2. Materials and method

2.1. Animals and housing

P60 CD1 male mice were divided into three groups: the sham group (craniotomy without dura mater disruption, n = 20), the control group (microinjection with vehicle solution, n = 20) and the experimental group (microinjection with gold nanoparticles (85×10^6/nl, n = 20). Then, animals of each group were divided into five sub-groups per time-point (n = 4 each), i.e., 3, 7, 14, 30, and 90 days after intracerebral injection. All these experimental procedures were approved and supervised by the Committee of Animal Care and Use of the University of Colima by following Mexican legal regulations (NOM-062-ZOO 1999) and N.I.H. guidelines.

2.2. Synthesis and characterization of GNPs

Synthesis and characterization of GNPs were done following a protocol previously described (González-Pedroza et al., 2017). The GNPs were synthesized using the citrate reduction method from a colloidal suspension of 1% $HAuCl_4$ (Sigma, Cat. W302600). First, 100 mL of deionized water were heated to boiling point and 5 mL of 0.05 M sodium citrate (Sigma, Cat. W302600) solution were added and stirred for 20 min. A red solution was obtained and 0.5 mL of 1 % polyethylene glycol (PEG; Sigma, Cat. 81300, MW = 4000) was then added and stirred for 10 min to prevent aggregation. PEG-GNPs were collected by centrifugation at 16,000 rpm for 30 min, washed twice with distilled water, and stored at 4 °C (Zhang et al., 2012; Kim et al., 2007).

We determined the optical properties of GNPs with UV–vis spectroscopy (Varian Cary 5000 UV–vis-NIR, Agilent Technologies, UK). Briefly, 1 mL of GNPs or 1 mL of PEG-GNPs was diluted in 1 mL of deionized water. Each sample was analyzed in a range of 200–800 nm in the absorption mode. These PEGylated GNPs were then analyzed by Transmission Electron Microscopy (TEM) (JEOL-2100 200 kV with LaB6 filament, Japan). Approximately, 50 μL of GNPs and GNPs-PEG were placed on grids and dried at room temperature for 20 min before TEM analysis. Quantitative analysis of the size of GNPs was performed by measuring the core diameter of 600 single nanoparticles of multiple micrographs and high-resolution transmission electron microscopy (HR-TEM).

2.3. Glass needles obtaining and preparation for microinjection

Glass needles were made with capillary glass tubes of 1–5 μl (Drummond; Wiretrol, Cat. 5-000-1001) by heating (2.90 V) and stretching in a Vertical Pipette Puller (Stoelting, No. 51210) as previously described (Gonzalez-Perez et al., 2010). The needle tip was cut and beveled until a 25–30-μm inner diameter tip was obtained. Then, the needle was secured in a microinjector holder (Narishige; Mod. MO-10) attached to a stereotactic device (RWD Life Science).

2.4. Microinjection of GNPs

Intracerebral injections were done by following a previously described procedure (Gonzalez-Perez et al., 2010). All animals were anesthetized with ketamine (90 mg/kg i.p. PiSA®) plus xylazine (10 mg/kg i.p. PiSA®). The mouse head was shaved and secured in a stereotactic device (RWD Life Science) and head skin was cleaned with an antiseptic solution (Microdacyn™, Oculus) and a longitudinal incision was done with a surgical blade from the interaural line to the Lambda line. A cotton swap was used to pull the skin out of the surgical field. We then set the anterior-posterior and lateral coordinates (0 mm and −2 mm from Bregma, respectively) (Paxinos and Franklin, 2004). At these coordinates, the skull was carefully drilled. We introduced a pre-loaded glass needle with GNPs or vehicle solution into the striatum (Z coordinate = −2.5 mm) and injected 100 nl of GNPs (85×10^6/nl) or vehicle solution at rate of 1 nl/sec. To minimize solution reflux, we kept the needle into the brain for two minutes. After needle removal, the wound skin was closed with surgical glue (Vetbond™). For anesthesia recovery, all animals were placed in a clean pre-warmed cage and received 5 mg/kg s.c. ketorolac (Senosiain) for post-surgical analgesia. The surgical procedure was done under a surgical microscope (Zeiss Surgical OPMI pico).

2.5. Tissue processing

Animals were anesthetized with sodium pentobarbital (50 mg/kg i.p. Pisabental™, PiSA). The transcardial perfusion was done with 0.9 % NaCl solution followed by 4 % paraformaldehyde (Sigma, Cat. P6148) dissolved in 0.1 M phosphate buffer and post-fixed overnight at 4 °C with the same fixative solution. We then cut 30-μm-thick coronal sections with a vibratome (Leica VT 1000S) between coordinates +1.50 mm and −1.50 mm (anterior-posterior from Bregma). These sections encompassed the injection site and perilesional area in the striatum.

2.6. Immunohistochemistry

Brain sections were rinsed three times for 10 min in 0.1 M PBS. Endogenous peroxidases were inactivated with 3% H_2O_2 dissolved in 0.1 M PBS for 30 min. The sections were then washed in 0.1 M PBS (10 min × 3) followed by incubation in a blocking solution (0.1 M PBS + 0.1 % Triton-X + 10 % fetal bovine serum) for 40 min at room temperature. Astrocytes were labeled with rabbit IgG anti-GFAP, dilution 1:1000 (Dako, Cat. Z0334), whereas microglia cells were labeled with rabbit IgG anti-Iba1, dilution 1:1000 (Wako, Cat. GR117789-10) incubated overnight at 4 °C in blocking solution. We then washed three times the brain sections with 0.1 M PBS for 10 min and incubated with biotinylated secondary antibody (anti-rabbit IgG + 0.1 M PBS + 10 % fetal bovine serum), dilution 1:200 for 60 min at room temperature in darkness. After, brain sections were washed with 0.1 M PBS (10 min × 3) and incubated in darkness with avidin-biotin complex (Vectastain ABC Kit, Elite Cat. PK-6101) for 60 min at room temperature. Brain sections were washed with 0.1 M PBS (10 min x 3) and the chemical reaction was revealed with 0.03 % 3,3'-diaminobenzidine (Aldrich, No. 261890) for 1 min. We washed all samples with 0.1 PBS (10 min x 3), mounted on glass slides, dehydrated and sealed with mounting medium (DPX Mounting Medium; Sigma, Cat. 06522).

2.7. Quantification and cytoplasmic transformation

To analyze astrocytes (GFAP + cells) or microglia cells (Iba1+ cells), at least five 30-μm thick brain sections were selected for each marker. These sections encompassed the lesion and perilesional area in the striatum (∼ 150 μm). We used a 40x objective (field area = 0.15 mm^2) and quantified only the cells with their

soma found in a single focal plane. We analyzed at least 80 focal planes per time point for each group. Astrocytic and microglia cytoplasmic transformation provides an estimation of reactive gliosis (Gonzalez-Perez et al., 2001). Cytoplasmic complexity was determined as described previously (Campos-Ordonez et al., 2015). We used a stereological grid, a template with 10 concentric circles (3.33 μm apart). From each group, we randomly selected 160 astrocytes and 160 microglia cells with clearly discernible nuclei in a single focal plane. Under a 40x magnification, we overlapped the stereological grid with every cell image. The cell body of astrocytes or microglia cells was placed in the central circle and the total number of intersecting points of cytoplasmic processes with the concentric grid lines were counted (Campos-Ordonez et al., 2015). These histological analyses were done in the perilesional site (0–500 μm) and brain parenchyma referred to as the distal region (500–1600 μm away from the injection site). All microphotographs and histological evaluations were done with a Zeiss Axio-Observer D1 optical microscope (Göttingen, Germany) and the Axio-Vision 4.8.1 acquisition Software (Göttingen, Germany).

2.8. Statistical analysis

All data are expressed as median and interquartile range (IQR: Q3 - Q1). We used the Mann-Whitney "*U*" test to determine differences between groups. The $p < 0.05$ value was selected to establish statistically significant differences.

3. Results

3.1. Gold nanoparticles synthesis and characterization

First, we characterized PEGylated GNPs and non-PEGylated GNPs by using UV/Vis analysis (Fig. 1A, curve 1). Our data indicated that PEGylated GNPs showed an emission peak of 523 nm, whereas non-PEGylated GNPs reached a plasmon resonance peak of 520 nanometers (Fig. 1A, curve 2). The number of peaks in the spectrum represents the morphology of the nanoparticles, in this case, a single peak suggested a spherical morphology (González-Pedroza et al., 2017; Liz-Marzán, 2004). Then, we did a TEM analysis to corroborate the morphology and size of PEGylated GNPs (Fig. 1B). Our findings indicated that the size of GNPs was 8.09 ± 3.60 nm (Fig. 1B, inset). TEM microscopy also confirmed the spherical form and narrow-size distribution of our nanoparticles (Fig. 1B). According to the file 004-0784 of the Joint Committee on Powder Diffraction Standards (JCPDS), the interplanar distance of GNPs was 2.08 Å, which indicates that GNPs have a crystalline structure that corresponds to the family of crystalline planes (200) (Fig. 1C).

3.2. Gold nanoparticles induces transient astrogliosis

A brain injury generates an increase in the number and cytoplasmic configuration of astrocytes, i.e. astrogliosis or reactive gliosis (Sofroniew, 2015; Bardehle et al., 2013). To evaluate the magnitude of astrogliosis that a single injection of PEGylated GNPs produced into the brain, we quantified the number of GFAP$^+$ cells and their cytoplasmic processes in the perilesional area and 500-μm outside the injection site ($n = 4$ per group) at all time points: 3-, 7-, 14-, 30-, and 90-day post-injection (Fig. 2). On day 3, we found a significant increase in the number of GFAP$^+$ cells in the GNPs group in comparison with the sham-operated group, but not with the control-vehicle (C–V) group (Fig. 3A). In the analysis of cytoplasmic transformation, we found a decrease in the number of grid intersections with GFAP$^+$ processes in the GNPs group when compared to the C–V group, but not with the sham group (Fig. 3B). We identified a minor increase in the cytoplasm complexity between the C–V group and the sham group, but no statistically significant differences were found (Table 1). At day 7 post-injection, we observed an important increase in the GFAP$^+$ cell population in the GNPs group in comparison with the sham group and the C–V group (Fig. 3A). Interestingly, no statistical differences were found in cytoplasmic transformation among all groups (Fig. 3B). At day 14 post-injection, the number of GFAP$^+$ cells remained high in the GNPs group as compared to the sham and the C–V group (Fig. 3A). In contrast, the number of intersections in the C–V group decreases in comparison to the sham group and the GNPs group. We did not find statistically significant differences between the sham and the GNPs groups (Fig. 3B and Table 1). At day 30 post-injection, the number of GFAP$^+$ cells in the GNPs group was still elevated when compared to the sham group and the C–V group (Fig. 3A). Interestingly, the number of grid-cell process intersections in the GNPs group was not statistically significant when compared to the sham group and the C–V group (Fig. 3B and Table 1). At day 90 post-injection, we observed that the number of GFAP$^+$ cells in the GNPs group was not statistically significant when compared to the sham group and the C–V group (Fig. 3A). A similar finding was found in the analysis of cytoplasmic complexity, where the GNPs group did not show significant differences as compared to the sham group and the C–V group (Fig. 3B and Table 1).

To determine whether astrogliosis was limited to the injection site or affected distal parenchymal regions, we analyzed astrogliosis parameters in the brain parenchyma (500 μm away from the injection site). Our data indicated that the number of astrocytes (Fig. 3C) and cytoplasmic transformation (Fig. 3D) showed similar patterns respect to the perilesional analysis, i.e. the GNP group showed a rapid increase in astrocytic response that reached control-vehicle levels on day 90 (Table 2). In summary, the astrocytic population increased in the first time points (3–7 DPI) but, eventually, it decreased and reached similar levels to those found in controls and no significant morphological changes were identified. To confirm our previous findings, we included an additional statistical analysis of morphometric data and compared the perilesional site and the distal brain parenchyma (Supplemental Table 1). On day 90, we found that GNP-induced astrocyte reactivity observed in the injection site did not show statistically significant differences as compared to distal regions. Interestingly, the C–V group did show statistically significant differences between these regions. Because the astrocytic response found between distal regions of the C–V and GNP groups was similar and the astrocytic response found in the injection site of the C–V group was higher than that found in the GNP group, we confirmed that GNPs produce fewer astrocytic response than the vehicle. Taken together, these findings suggest that astrogliosis induced by GNPs is transient and mostly self-limited.

3.3. Gold nanoparticles induces a transitory activation of microglia cells

Microglia cells contribute to glial scar formation and activate astrocyte response after brain damage (Liddelow et al., 2017; Adams and Gallo, 2018). To investigate whether a single administration of AuNP generated microglia activation, we analyzed the number and cytoplasmic transformation of microglia in the perilesional area and 500-μm outside the injection site ($n = 4$ per group) at all time points: 3-, 7-, 14-, 30-, and 90-day post-injection (Fig. 4). Three days after injection, the number of Iba1$^+$ cells in the GNPs group did not show a significant increase as compared to the C–V group (Fig. 5A). However, the GNPs group showed a certain trend toward significance when compared to the sham group (Table 3). The analysis of cytoplasmic complexity indicated that Iba1$^+$ cells exhibited a highly branched morphology in the GNPs group in comparison to the C–V group and the sham group (Fig. 5B). At day 7 post-injection, the number of Iba1$^+$ cells showed an important

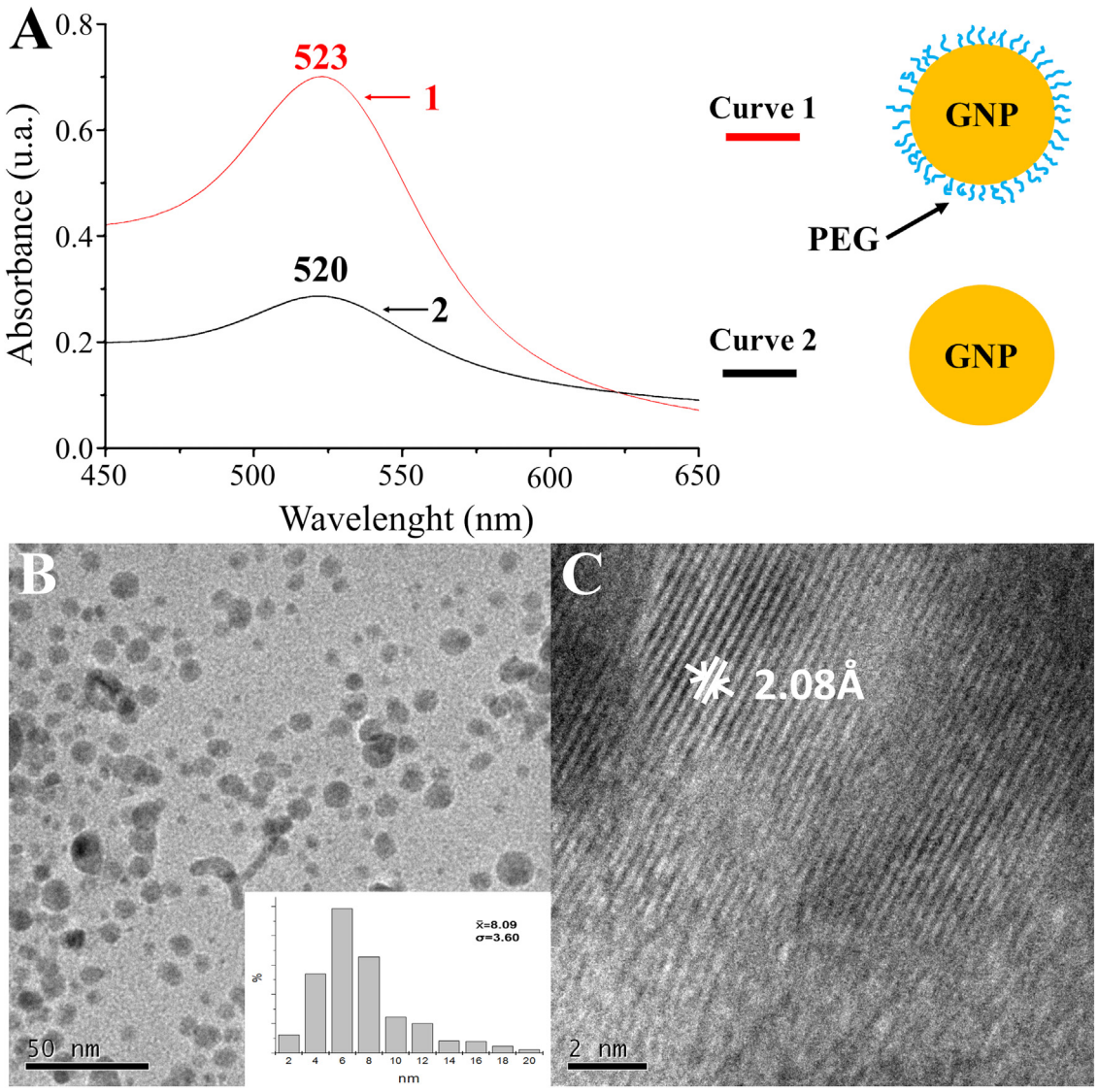

Fig. 1. UV–vis spectra and TEM observations of Gold nanoparticles (GNPs). **A.** PEGylated GNPs (curve 1) and non-PEGylated GNPs (curve 2). **B.** Micrograph of GNPs; inset shows the size distribution of nanoparticles, B) high resolution (HR-TEM) show an interplanar distance of 2.08 Å. Scale bar = 50 nm (**B**) and 2 nm (**C**).

Table 1
GFAP⁺ cells and their cytoplasmic transformation in the perilesional area after GNPs administration. Data are expressed as the median and interquartile range (IQR = Q3-Q1); Mann-Whitney "*U*" test. * $p < 0.05$. C-V: control vehicle group; GNPs: gold-nanoparticles group.

Time Point	Group	GFAP⁺ Cell Population				Group	GFAP⁺ Cell Intersections			
		M (Q3 – Q1)	Comparison (*versus*)	*U* test	*P* value		M (Q3 – Q1)	Comparison (*versus*)	*U* test	*P*value
3 DPI	Sham	2.10 (2.47–1.47)	C–V	0.000	*0.021	Sham	22.02 (24.65–18.27)	C–V	2.000	0.083
	C–V	22.72 (29.55–19.27)	GNPs	2.000	0.083	C–V	29.71 (33.47–25.96)	GNPs	0.000	*0.021
	GNPs	33.17 (40.20–29.07)	Sham	0.000	*0.021	GNPs	17.02 (18.97–14.95)	Sham	3.000	0.149
7 DPI	Sham	2.72 (2.02–2.60)	C–V	0.000	*0.021	Sham	22.90 (24.19–22.29)	C–V	8.000	1.000
	C–V	19.12 (27.35–15.95)	GNPs	1.000	*0.043	C–V	22.23 (28.42–17.00)	GNPs	8.000	1.000
	GNPs	43.02 (46.92–31.52)	Sham	0.000	*0.021	GNPs	22.12 (27.70–17.32)	Sham	8.000	1.000
14 DPI	Sham	1.70 (2.02–1.45)	C–V	0.000	*0.021	Sham	23.97 (26.61–22.61)	C–V	0.000	*0.021
	C–V	7.47 (8.37–5.50)	GNPs	0.000	*0.021	C–V	19.55 (19.74–19.24)	GNPs	0.000	*0.021
	GNPs	36.25 (39.07–32.70)	Sham	0.000	*0.021	GNPs	21.81 (23.34–20.76)	Sham	3.000	0.149
30 DPI	Sham	3.00 (3.57–2.05)	C–V	0.000	*0.021	Sham	20.70 (22.65–20.21)	C–V	1.000	*0.043
	C–V	14.85 (16.97–11.05)	GNPs	0.000	*0.021	C–V	26.23 (27.45–23.74)	GNPs	2.000	0.114
	GNPs	31.37 (35.35–26.62)	Sham	0.000	*0.021	GNPs	21.12 (24.74–17.52)	Sham	8.000	1.000
90 DPI	Sham	4.47 (5.60–3.42)	C–V	0.000	*0.021	Sham	22.58 (23.92–20.89)	C–V	4.000	0.248
	C–V	12.67 (17.67–8.42)	GNPs	5.000	0.486	C–V	24.13 (25.22–22.60)	GNPs	5.000	0.386
	GNPs	8.90 (15.12–5.05)	Sham	2.500	0.110	GNPs	24.37 (28.43–23.53)	Sham	4.000	0.248

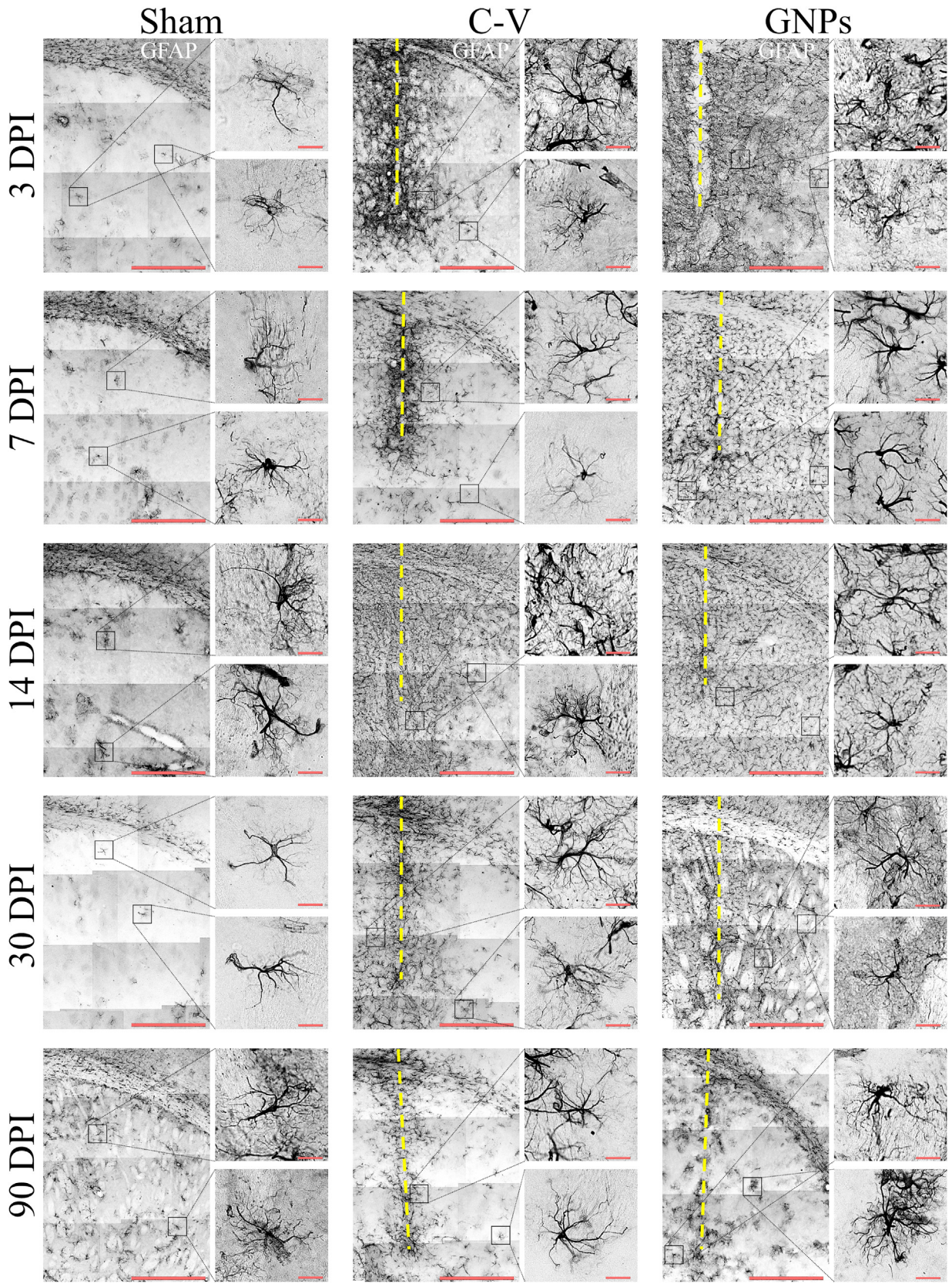

Fig. 2. Astrogliosis in the perilesional and distal area. Astrocytes (GFAP-expressing cells) in the sham-operated, control-vehicle (C-V) and GNPs groups at 3, 7, 14, 30, and 90 days post-injection (DPI). After GNPs injection, the number of astrocytes increases since day 3 and remains elevated for 30 days, until it decreases on day 90 after GNPs administration. Larger images show the injection site where needle track was identified (dotted lines). Insets show cells found in the perilesional area (0–550 μm; upper panels) or distal areas (500 - 1600 μm; lower panels). Scale bar =500 μm; inset scale bar =20 μm.

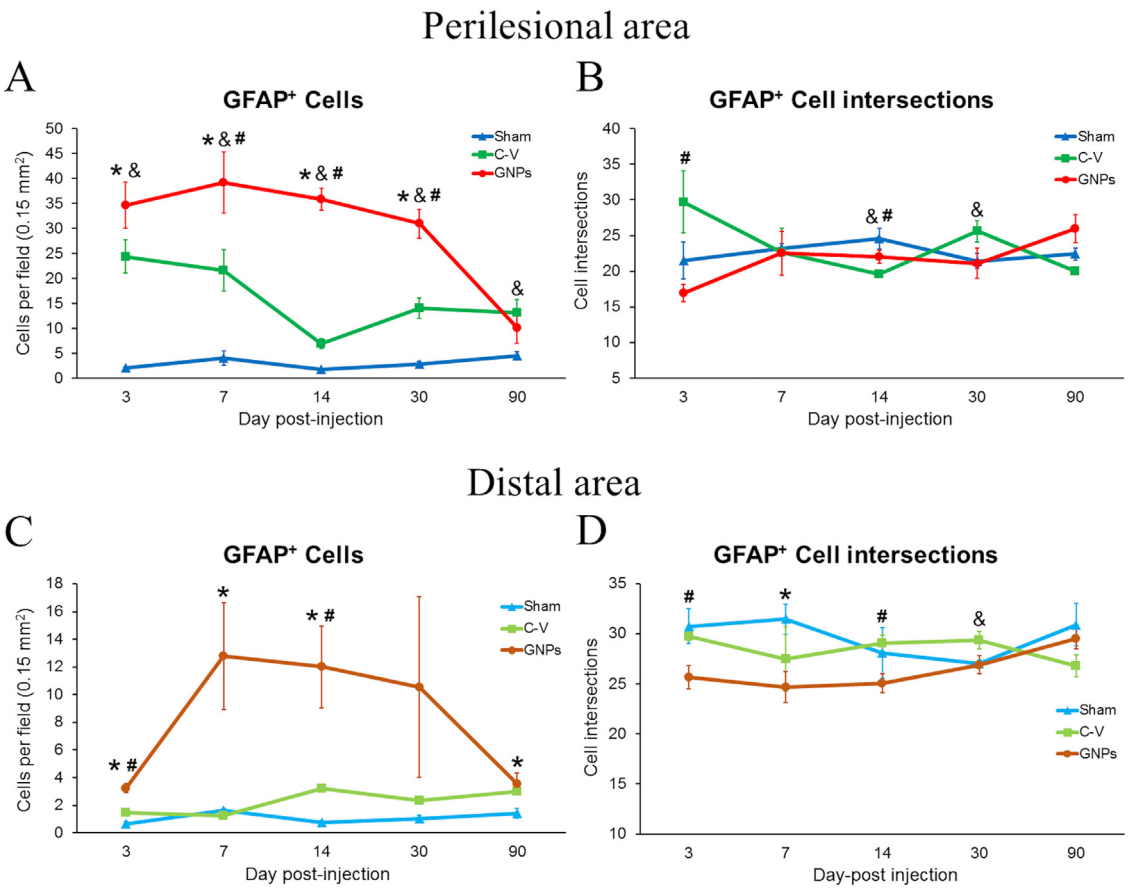

Fig. 3. Gold-nanoparticles (GNPs) produce transitory astrogliosis. **A.** Around the injection site, astrocyte population decreases to reach basal levels on day 90 in the GNPs groups. **B.** The cytoplasmic complexity of astrocytes appeared to be unaffected around the needle track in all time points. **C.** Astrocytes population quantified in distal regions (500-1600 μm away from the injection site). The GNPs group showed a transient increase that reached the levels of the C-V group. **D.** The cytoplasmic complexity in distal areas was unaffected in all groups. Data are expressed as the mean and ES; $n = 4$. Symbols (*, & and #) represents $P < 0.05$; Mann-Whitney "*U*" test. * (Sham vs. GNPs); & (Sham vs. C-V); # (C-V vs. GNPs).

Table 2
GFAP⁺ cells and their cytoplasmic transformation in the distal area after GNPs administration. Data are expressed as the median and interquartile range (IQR = Q3-Q1); Mann-Whitney "*U*" test. * $p < 0.05$. C-V: control vehicle group; GNPs: gold-nanoparticles group.

Time Point	Group	GFAP⁺ Cell Population				Group	GFAP⁺ Cell Intersections			
		M (Q3 – Q1)	Comparison (*versus*)	*U* test	*P* value		M (Q3 – Q1)	Comparison (*versus*)	*U* test	*P* value
3 DPI	Sham	0.66 (0.93–0.36)	C–V	2.000	0.083	Sham	31.27 (32.83–28.62)	C–V	4.000	0.248
	C–V	1.30 (1.93–0.93)	GNPs	1.000	*0.043	C–V	29.55 (30.36–29.03)	GNPs	0.000	*0.021
	GNPs	3.39 (3.69–2.73)	Sham	0.000	*0.021	GNPs	26.00 (27.20–24.14)	Sham	2.000	0.083
7 DPI	Sham	1.49 (1.79–1.43)	C–V	7.000	0.773	Sham	31.39 (33.64–29.20)	C–V	6.000	0.564
	C–V	1.26 (1.99–0.49)	GNPs	2.000	0.083	C–V	27.22 (33.00–21.87)	GNPs	6.000	0.564
	GNPs	14.86 (17.30–8.23)	Sham	1.000	*0.043	GNPs	25.20 (26.74–22.63)	Sham	1.000	*0.043
14 DPI	Sham	0.83 (0.96–0.57)	C–V	4.000	0.248	Sham	21.12 (31.20–24.97)	C–V	4.000	0.248
	C–V	1.23 (2.76–0.69)	GNPs	0.000	*0.021	C–V	29.04 (30.35–27.68)	GNPs	1.000	*0.043
	GNPs	10.06 (15.78–8.19)	Sham	0.000	*0.021	GNPs	24.72 (26.51–23.54)	Sham	6.000	0.564
30 DPI	Sham	1.01 (1.34–0.71)	C–V	1.500	0.059	Sham	27.17 (27.43–26.55)	C–V	1.000	*0.043
	C–V	2.03 (3.16–1.46)	GNPs	3.500	0.191	C–V	29.21 (30.46–28.25)	GNPs	3.000	0.149
	GNPs	5.63 (18.33–2.73)	Sham	1.500	0.059	GNPs	26.43 (28.06–25.66)	Sham	6.000	0.564
90 DPI	Sham	1.10 (1.83–1.00)	C–V	2.000	0.081	Sham	30.71 (34.56–27.20)	C–V	2.000	0.083
	C–V	3.16 (4.29–1.66)	GNPs	7.000	0.773	C–V	26.24 (28.56–25.44)	GNPs	3.000	0.149
	GNPs	3.16 (4.59–2.43)	Sham	1.000	*0.042	GNPs	28.69 (30.75–28.19)	Sham	8.000	1.000

increase in the GNPs group regarding the sham group (Fig. 5A and Table 3). Remarkably, gold-nanoparticles only produced a marginal significance in the microglia response when compared to the C–V group. Interestingly, we did not find statistically significant differences in the cytoplasmic transformation of microglia cells among groups (Fig. 5B and Table 3). At day 14 post-injection, the number of microglia cells in the GNPs group showed an important decrease that reached similar levels to those found in the other groups (Fig. 5A). The morphology of Iba1⁺ cells seemed to remain unchanged in mice with GNPs as compared to the sham group and the C–V group. At this time point, statistically significant differences were only found between the sham and the C–V group (Fig. 5B and Table 3). At day 30 post-injection, the number of microglia cells did not show statistically significant differences among all groups

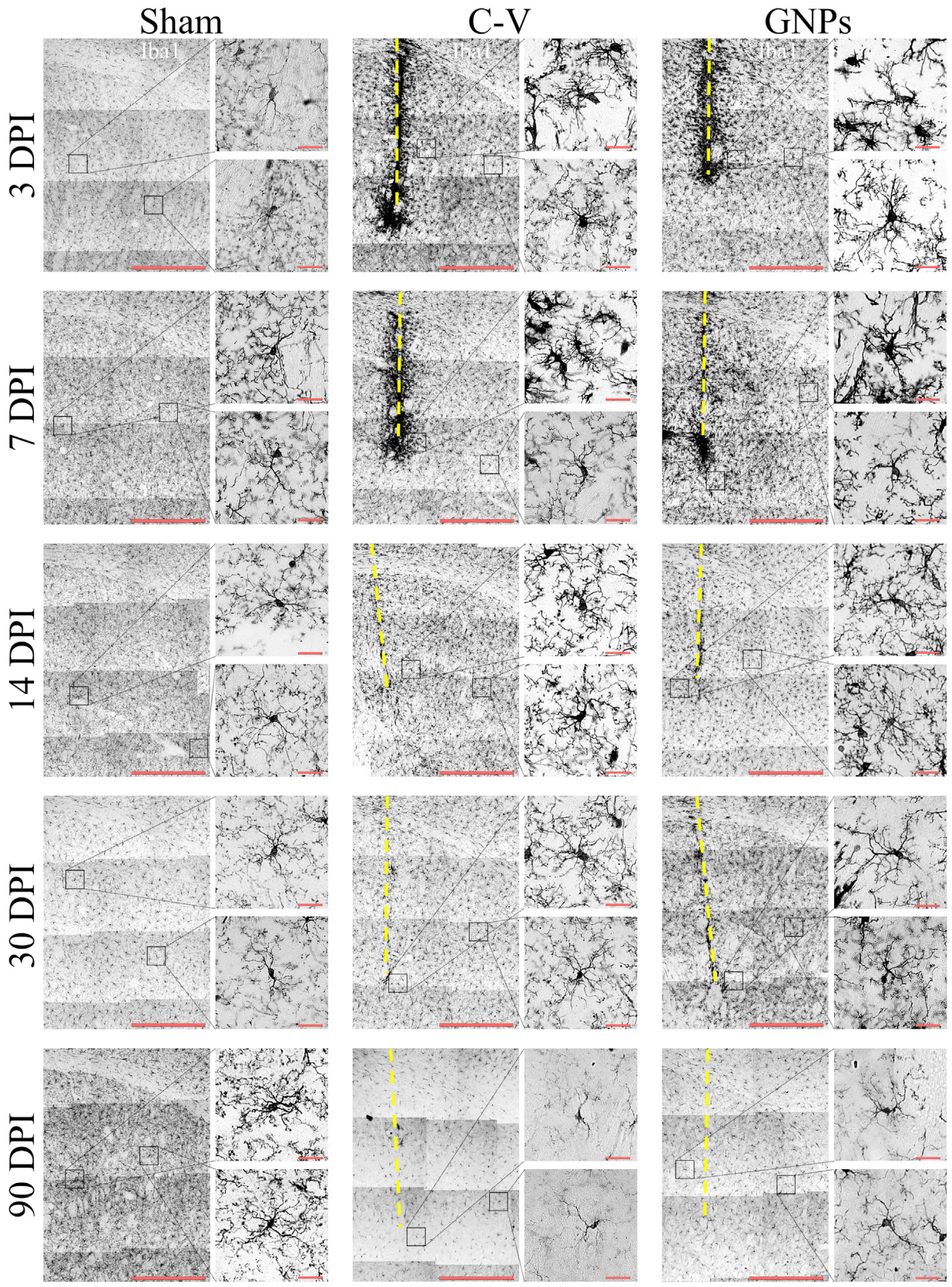

Fig. 4. Microglia response after GNPs injection. Microglia cells (Iba1-expressing cells) found at 3, 7, 14, 30, and 90 days post-injection. After the GNPs injection, the population of microglial cells increases significantly on day 7 and decreases progressively on day 14 to remain stable until day 90. Morphologic changes were evident only at 3rd day post-injection. These changes were not evident in the following time points. Larger images show the injection site where needle track was identified (dotted lines). Insets show cells found in the perilesional area (0–550 μm; upper panels) or distal areas (500–1600 μm; lower panels). Scale bar =500 μm; inset scale bar =20 μm.

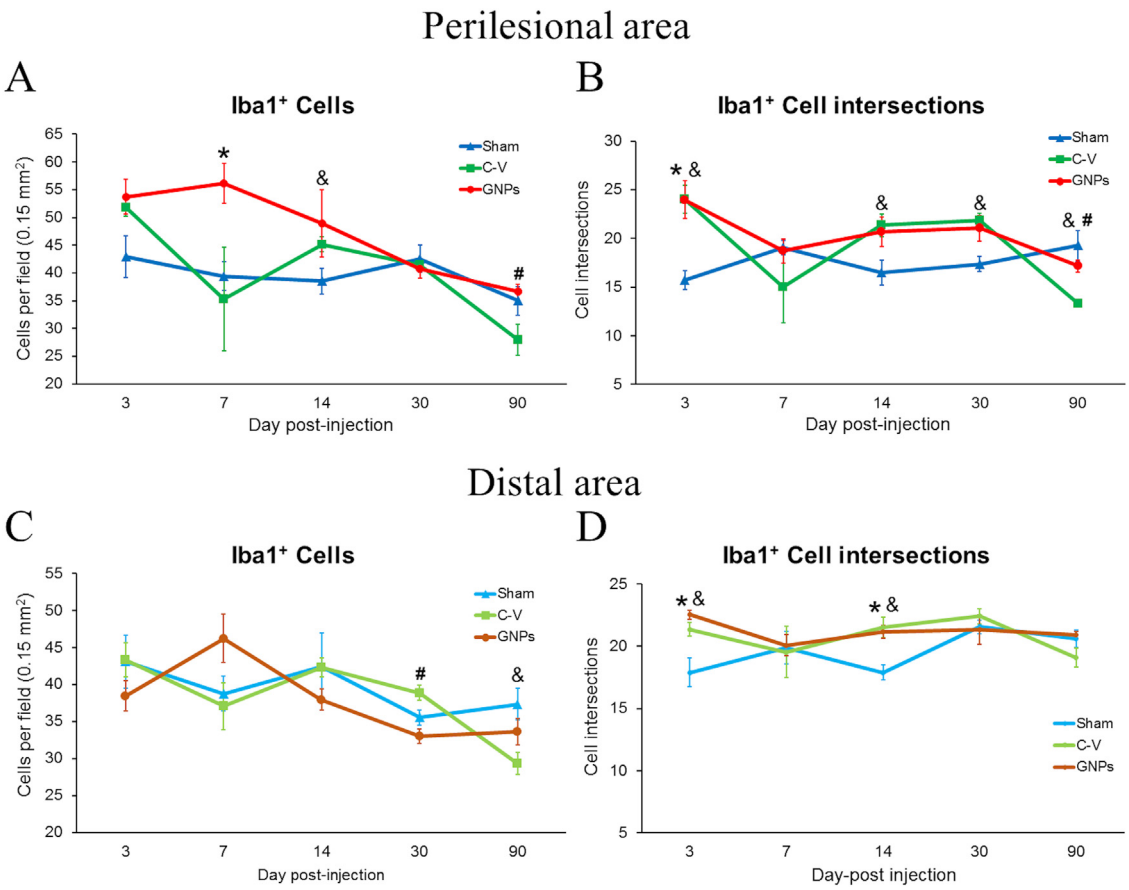

Fig. 5. Microgliosis in the injection site and distal areas. **A.** Around the injection site, the number of microglia cells (Iba1⁺ cells) of the GNPs group normalizes on day 14. **B.** Morphologic changes of microglia cells are evident only on day 3. **C.** In the distal area (500–1600 μm away from the injection site), microglia cells appeared to be unaffected by GNPs. **D.** Morphologic changes of distal microglia cells are present only from day 3 to day 14 after GNPs administration. Data are expressed as the mean and ES; $n = 4$. Symbols (*, & and #) represents $P < 0.05$; Mann-Whitney "*U*" test. * (Sham vs. GNPs); & (Sham vs. C-V); # (C-V vs. GNPs).

Table 3
Iba1⁺ cells and their cytoplasmic transformation in the perilesional area after gold nanoparticle administration. Data are expressed as the median and interquartile range (IQR = Q3-Q1); Mann-Whitney "*U*" test. * $p < 0.05$. C-V: control vehicle group; GNPs: gold-nanoparticles group.

Time Point	Group	Iba1⁺ Cell Population				Group	Iba1⁺ Cell Intersections			
		M (Q3 – Q1)	Comparison (*versus*)	*U* test	*P* value		M (Q3 – Q1)	Comparison (*versus*)	*U* test	*P* value
3 DPI	Sham	42.20 (49.35–36.60)	C–V	2.000	0.083	Sham	16.31 (16.83–14.57)	C–V	0.000	*0.021
	C–V	51.60 (54.25–49.32)	GNPs	2.000	0.083	C–V	25.06 (25.84–22.20)	GNPs	7.000	0.773
	GNPs	52.02 (58.35–49.15)	Sham	7.000	0.773	GNPs	22.72 (26.07–21.28)	Sham	0.000	*0.021
7 DPI	Sham	38.27 (42.67–36.20)	C–V	8.000	1.000	Sham	18.71 (20.02–18.11)	C–V	7.000	0.773
	C–V	33.90 (51.37–19.17)	GNPs	2.000	0.083	C–V	14.85 (21.41–8.58)	GNPs	7.000	0.773
	GNPs	54.92 (61.55–50.67)	Sham	0.000	*0.021	GNPs	19.09 (20.58–16.82)	Sham	8.000	1.000
14 DPI	Sham	38.22 (41.65–35.35)	C–V	1.000	*0.043	Sham	17.22 (18.06–14.89)	C–V	0.000	*0.021
	C–V	45.27 (47.07–43.25)	GNPs	4.000	0.248	C–V	20.76 (23.10–19.58)	GNPs	7.000	0.083
	GNPs	51.57 (57.32–40.47)	Sham	4.000	0.248	GNPs	20.58 (22.73–18.65)	Sham	2.000	0.773
30 DPI	Sham	42.00 (46.05–39.10)	C–V	7.000	0.773	Sham	16.93 (18.53–16.22)	C–V	0.000	*0.021
	C–V	41.20 (42.52–40.45)	GNPs	8.000	1.000	C–V	22.36 (22.91–20.78)	GNPs	6.000	0.686
	GNPs	41.15 (43.50–37.85)	Sham	7.000	0.773	GNPs	20.82 (23.13–18.93)	Sham	2.000	0.083
90 DPI	Sham	34.25 (38.32–31.60)	C–V	2.000	0.083	Sham	18.99 (21.88–16.61)	C–V	0.000	*0.021
	C–V	29.37 (32.00–23.80)	GNPs	0.000	*0.021	C–V	13.26 (13.92–12.73)	GNPs	0.000	*0.021
	GNPs	36.60 (38.82–34.35)	Sham	6.000	0.564	GNPs	17.01 (16.17–18.12)	Sham	5.000	0.386

(Fig. 5A). Besides, the number of Iba1⁺ intersections in the GNPs group did not show statistical significance (Table 3). At day 90 post-injection, the Iba1⁺ cells in the GNPs group showed statistical differences in comparison to the C–V group (Fig. 5A). Remarkably, the GNPs group did not show significant differences when compared to the sham-operated group (Fig. 5A). The number of the grid-cell process intersections did not show statistical differences between the GNPs and the sham-operated groups but, the C–V group showed significant differences when compared to the other groups (Table 3).

To determine whether microglia activation was restricted to the injection site or affected parenchymal regions, we analyzed the microglia cell population within brain parenchyma (500 μm away from the injection site). We found that the number of microglia cells increased on day7 in the GNP group, but it returns to basal levels from day 14 (Fig. 5C). In contrast,

Table 4
Iba1⁺ cells and their cytoplasmic transformation in the distal area after GNPs administration. Data are expressed as the median and interquartile range (IQR = Q3-Q1); Mann-Whitney "*U*" test. * $p < 0.05$. C-V: control vehicle group; GNPs: gold-nanoparticles group.

Time Point	Group	Iba1⁺ Cell Population				Group	Iba1⁺ Cell Intersections			
		M (Q3 – Q1)	Comparison (*versus*)	*U* test	*P* value		M (Q3 – Q1)	Comparison (*versus*)	*U* test	*P* value
3 DPI	Sham	42.40 (47.50–38.63)	C–V	8.000	1.000	Sham	18.76 (19.40–16.36)	C–V	0.000	*0.021
	C–V	42.39 (46.36–40.29)	GNPs	4.000	0.248	C–V	21.71 (22.06–20.63)	GNPs	3.500	0.191
	GNPs	37.43 (41.46–35.39)	Sham	5.000	0.236	GNPs	22.36 (23.13–21.91)	Sham	0.000	*0.021
7 DPI	Sham	38.06 (41.69–35.76)	C–V	6.500	0.663	Sham	19.65 (21.65–18.13)	C–V	7.000	0.773
	C–V	38.03 (42.36–31.76)	GNPs	2.000	0.083	C–V	20.21 (22.84–16.22)	GNPs	7.000	0.773
	GNPs	46.06 (51.40–41.03)	Sham	2.000	0.083	GNPs	20.76 (19.01–21.14)	Sham	6.000	0.564
14 DPI	Sham	41.83 (48.66–36.13)	C–V	8.000	1.000	Sham	17.80 (18.85–16.94)	C–V	0.000	*0.021
	C–V	41.73 (44.26–40.33)	GNPs	2.000	0.083	C–V	21.35 (22.73–20.31)	GNPs	7.000	0.773
	GNPs	37.40 (39.70–36.16)	Sham	5.000	0.386	GNPs	20.91 (21.91–20.36)	Sham	0.000	*0.021
30 DPI	Sham	35.36 (37.26–33.73)	C–V	2.000	0.083	Sham	21.73 (22.31–20.79)	C–V	5.000	0.386
	C–V	38.89 (40.33–37.36)	GNPs	0.000	*0.021	C–V	22.35 (23.36–21.45)	GNPs	5.500	0.468
	GNPs	32.96 (34.46–31.50)	Sham	3.000	0.149	GNPs	21.28 (23.33–19.33)	Sham	8.000	1.000
90 DPI	Sham	36.96 (40.60–34.06)	C–V	0.000	*0.021	Sham	21.13 (21.44–19.75)	C–V	4.000	0.248
	C–V	30.46 (31.00–27.53)	GNPs	3.000	0.149	C–V	18.75 (20.03–18.14)	GNPs	3.000	0.149
	GNPs	34.78 (36.03–31.23)	Sham	5.000	0.386	GNPs	20.71 (21.21–20.55)	Sham	7.000	0.773

The analysis of cytoplasmic transformation indicated that the C–V group and GNPs had similar patterns and both of them reached the control level on day 30 (Fig. 5D). The numerical data and summary statistics are shown in Table 4. As done for astrocytic analysis, we compared the microglia response in the injection site vs. distal regions in all time points (Supplemental Table 2). In general, we found that microglial reactivity did not show statistically significant differences between the injection site and distal regions, which suggests that microglial response was mainly circumscribed to the injection site and it remained stable throughout the study. Altogether, our results showed that the cellular immune response induced by the intracerebral injection of gold nanoparticles is self-limited, decays rapidly, and is primarily confined to the injection site, predominantly.

4. Discussion

To the best of our knowledge, this is the first study that analyses the long-term effects of GNPs delivered into the brain on the glial response. Herein, we show that the intracerebral injection of spherical GNPs increases the number of astrocytes and microglia cells, and their cytoplasmic complexity in the perilesional area. Remarkably, these cellular changes are transient, moderate and predominantly circumscribed to the injection site. The cellular enlargement, the high cytoplasmic complexity, and the increase in glial populations are suggestive of reactive gliosis (Sofroniew, 2015; Bardehle et al., 2013; Adams and Gallo, 2018; Liddelow et al., 2017), which are indirect indicators of the magnitude of a brain insult (Sofroniew, 2009; Sofroniew and Vinters, 2010). Therefore, our data indicate that GNPs produce a very limited tissue disruption in the brain homeostasis.

The cellular response and cytotoxicity of GNPs not only depends on the size, shape, and other physical properties of each nanoparticle but also on the targeted tissue (Madhusudanan et al., 2017; Rizvi et al., 2018). GNPs may trigger cytotoxic responses in a size-dependent manner in several cell types (Pan et al., 2009, 2007; Xia et al., 2019), and the cytotoxic mechanism is triggered by caspase-3, oxidative stress, mitochondrial disruption, cytokine releasing (IL-6 and IL-1a) and overexpression of TLR-2 (Pan et al., 2009, 2007; Xia et al., 2019). In the brain, small GNPs (diameter ≤ 5 nm) can induce strong glial reactivity in the cortex (Lee et al., 2016; Liu et al., 2013b) and enhance the damage progression of cerebral ischemia in rats (Liu et al., 2013b). In our study, we used 8-nm GNPs and evaluated the glial response in the long-term at different time points. We observed that the astroglial response increased on day 3 and reached its highest point on day 7; eventually, astroglial response reaches a plateau between days 14 and 30 that finally normalizes on day 90. These findings indicate that GNPs produces a transient increase in astrocytic population. In the brain parenchyma located 500 μm away from the injection site, these cellular events showed very similar a time course, which confirms that GNPs produces a transitory and limited astroglial response in the adult brain. We did not find statistically significant differences at the final time point (day 90) between the C–V and GNP group in astrogliosis, which supports the notion that glial reactivity found in the GNP group was mainly due to the surgical manipulation.

We used GFAP expression to label astrocytes, GFAP is an intermediate filament protein that is overexpressed in astrocytes after damage (Hol and Pekny, 2015). Interestingly, the analysis of cytoplasmic transformation showed that astrocytes had fewer processes when GNPs were injected and acquired a normal morphology from day 7 to the end of the study, which suggests that 8-nm GNPs *per se* did not produce an additional glial response (Fig. 4B). These beneficial effects of GNPs have been associated with a high expression of anti-apoptotic genes, IL-10, IL-4, and NF-κB, as well as a decrease in the expression of pro-apoptotic genes and TNF-α levels (Liu et al., 2013b; Mytych et al., 2015). However, these effects are not desirable for all body organs and tissue cells, in consequence, the local administration of GNPs may be mandatory to avoid the spread of GNPs throughout the body.

Microglia cells are the first line of defense against brain damage by increasing their phagocytic activity (Li and Barres, 2018). Thus, the level of microglia activity may reflect the magnitude of damage to the brain. Microglia cells can uptake GNPs without compromising their viability (Ji et al., 2019; Stojiljković et al., 2016; Hutter et al., 2010). The capacity of microglia for internalizing GNPs depends on the formation of the protein corona surrounding the GNPs (Kuschnerus et al., 2020). The protein corona is formed when the GNPs enter in a biological medium (García-Álvarez et al., 2018) and increase the GNPs uptake by microglia (Kuschnerus et al., 2020). PEG prevents aggregation and formation of a prominent protein corona that, in turn, inhibits cellular uptake (González-Pedroza et al., 2017; Mosquera et al., 2018). We found that upon intracerebral injection of PEGylated-GNPs, the number of microglia increases and peaks on day 7 and tend to normalize in all subsequent time points (Fig. 4C). Microglia cells acquire a highly branched morphology with an enlarge soma at 3 days, but this cellular enlargement is normalized at 7 days (Fig. 4D). This evidence indicates that microgliosis is transient and turns to basal levels faster than astrocytes, which may limit the

pro-inflammatory microenvironment in the brain. Our results also showed that microglia response observed in distal brain regions (550–1600 μm) very limited and brief, which suggests that GNPs did not significantly increases the immunological response mediated by microglia cells.

There are different types of metallic nanoparticles such as iron oxide, titanium dioxide, zinc oxide, and silver nanoparticles, which seem to be more toxic than GNPs for the neural tissue because they promote Fe^{2+} releasing (Luther et al., 2013), increase the levels of reactive oxygen species (Petters et al., 2016), and promote autophagy with mitochondrial damage (Long et al., 2006; Wilson et al., 2015; Pérez-Arizti et al., 2020; Wang et al., 2014; Sharma et al., 2017; Song et al., 2019). These pathological changes are mediated by microglia cells that release IL-6, IL-1β, and TNF-α (Xue et al., 2012; Liu et al., 2013a). In our study, the microglia population was increased in the GNPs' group, but only between the third and seventh days. Most importantly, GNPs did not induce a chronic microglia response as observed on days 30 and 90. This evidence contrasts with that obtained with silver nanoparticles that compromise the cell viability (Luther et al., 2011, 2012), activate microglia cells (Huang et al., 2015; Xu et al., 2015), and induce oxidative stress (Sun et al., 2016; Haase et al., 2012). Thus, our findings suggest that GNPs induce either a transitory pro-inflammatory microenvironment or activate anti-inflammatory mechanisms *in vivo* as suggested with *in-vitro* approaches (Liu et al., 2013b; Mytych et al., 2015). Interestingly, the type of polymer coat and shape of GNPs seem to be crucial to trigger the microglia response as observed in the olfactory bulb of adult mice (Hutter et al., 2010). Our findings confirmed that PEGylated and spherical GNPs produce a limited expression of Iba1+ cells in the long term. Besides, PEGylated and spherical GNPs are slowly internalized by microglia cells as compared to other shapes or polymer coats (Hutter et al., 2010). A slow clearance of PEGylated GNPs allows them to remain in the brain parenchyma, which is a crucial characteristic for the design of long-lasting pharmaceutical vehicles.

In summary, the intracerebral administration of GNPs produces transitory and self-limited astrogliosis and microgliosis. This evidence indicates that GNPs have low deleterious effects for the brain and may be suitable candidates for pharmacological applications, specifically as drug reservoirs/carriers for the treatment of neurological diseases. Thus, GNPs may be a promising pharmacological vehicle for delivering long-lasting drugs into the brain.

CRediT authorship contribution statement

Eduardo Lira-Diaz: Investigation, Methodology, Validation, Formal analysis, Writing - original draft. **Maria G. Gonzalez-Pedroza:** Methodology, Investigation. **Clemente Vasquez:** Resources, Writing - review & editing. **Raul A. Morales-Luckie:** Supervision, Resources, Funding acquisition. **Oscar Gonzalez-Perez:** Writing - review & editing, Supervision, Project administration, Resources, Funding acquisition.

Declaration of Competing Interest

None.

Acknowledgements

This study was financed by grants from Consejo Nacional de Ciencia y Tecnologia (CONACyT: 2015-01-465) to O.G-P and CONACyT's fellowship grant to E.L-D (No. 736004).

Appendix A. Supplementary data

Supplementary material related to this article can be found, in the online version, at doi:https://doi.org/10.1016/j.neures.2020.12.003.

References

Adams, K.L., Gallo, V., 2018. The diversity and disparity of the glial scar. Nat. Neurosci. 21, 9.
Amoozgar, Z., Yeo, Y., 2012. Recent advances in stealth coating of nanoparticle drug delivery systems. Wiley Interdiscip. Rev. Nanomed. Nanobiotechnol. 4, 219–233.
ASTM, E., 2006. 2456-06 "terminology for nanotechnology". ASTM Int., 2.
Austin, L.A., Mackey, M.A., Dreaden, E.C., El-Sayed, M.A., 2014. The optical, photothermal, and facile surface chemical properties of gold and silver nanoparticles in biodiagnostics, therapy, and drug delivery. Arch. Toxicol. 88, 1391–1417.
Bardehle, S., Kruger, M., Buggenthin, F., Schwausch, J., Ninkovic, J., Clevers, H., Snippert, H.J., Theis, F.J., Meyer-Luehmann, M., Bechmann, I., Dimou, L., Gotz, M., 2013. Live imaging of astrocyte responses to acute injury reveals selective juxtavascular proliferation. Nat. Neurosci. 16, 580–586.
Burda, J.E., Sofroniew, M.V., 2014. Reactive gliosis and the multicellular response to CNS damage and disease. Neuron 81, 229–248.
Campos-Ordonez, T., Zarate-Lopez, D., Galvez-Contreras, A.Y., Moy-Lopez, N., Guzman-Muniz, J., Gonzalez-Perez, O., 2015. Cyclohexane produces behavioral deficits associated with astrogliosis and microglial reactivity in the adult hippocampus mouse brain. Cell. Mol. Neurobiol. 35, 503–512.
Elahi, N., Kamali, M., Baghersad, M.H., 2018. Recent biomedical applications of gold nanoparticles: a review. Talanta 184, 537–556.
García-Álvarez, R., Hadjidemetriou, M., Sánchez-Iglesias, A., Liz-Marzán, L.M., Kostarelos, K., 2018. In vivo formation of protein corona on gold nanoparticles. The effect of their size and shape. Nanoscale 10, 1256–1264.
González-Pedroza, M.G., Sánchez-Mendieta, V., Morales-Valencia, J.A., López-Téllez, G., Argueta-Figueroa, L., González-Pérez, O., Morales-Luckie, R.A., 2017. Study X-ray photoelectron spectroscopy determination of interactions between gold nanoparticles and epidermal growth factor for potential use in biomedicine. J. Bionanoscience 11, 1–7.
Gonzalez-Perez, O., Ramos-Remus, C., Garcia-Estrada, J., Luquin, S., 2001. Prednisone induces anxiety and glial cerebral changes in rats. J. Rheumatol. 28, 2529–2534.
Gonzalez-Perez, O., Guerrero-Cazares, H., Quinones-Hinojosa, A., 2010. Targeting of deep brain structures with microinjections for delivery of drugs, viral vectors, or cell transplants. J. Vis. Exp.
Haase, A., Rott, S., Mantion, A., Graf, P., Plendl, J., Thünemann, A.F., Meier, W.P., Taubert, A., Luch, A., Reiser, G., 2012. Effects of silver nanoparticles on primary mixed neural cell cultures: uptake, oxidative stress and acute calcium responses. Toxicol. Sci. 126, 457–468.
Hol, E.M., Pekny, M., 2015. Glial fibrillary acidic protein (GFAP) and the astrocyte intermediate filament system in diseases of the central nervous system. Curr. Opin. Cell Biol. 32, 121–130.
Howard, M.D., Jay, M., Dziubla, T.D., Lu, X., 2008. PEGylation of nanocarrier drug delivery systems: state of the art. J. Biomed. Nanotechnol. 4, 133–148.
Huang, C.-L., Hsiao, I.-L., Lin, H.-C., Wang, C.-F., Huang, Y.-J., Chuang, C.-Y., 2015. Silver nanoparticles affect on gene expression of inflammatory and neurodegenerative responses in mouse brain neural cells. Environ. Res. 136, 253–263.
Hutter, E., Boridy, S., Labrecque, S., Lalancette-Hebert, M., Kriz, J., Winnik, F.M., Maysinger, D., 2010. Microglial response to gold nanoparticles. ACS Nano 4, 2595–2606.
Ji, J., Moquin, A., Bertorelle, F., Ky Chang, P., Antoine, R., Luo, J., Mckinney, R.A., Maysinger, D., 2019. Organotypic and primary neural cultures as models to assess effects of different gold nanostructures on glia and neurons. Nanotoxicology 13, 285–304.
Kim, D., Park, S., Lee, J.H., Jeong, Y.Y., Jon, S., 2007. Antibiofouling polymer-coated gold nanoparticles as a contrast agent for in vivo X-ray computed tomography imaging. J. Am. Chem. Soc. 129, 7661–7665.
Kuschnerus, I., Lau, M., Giri, K., Bedford, N., Biazik, J., Ruan, J., Garcia-Bennett, A., 2020. Effect of a protein corona on the fibrinogen induced cellular oxidative stress of gold nanoparticles. Nanoscale 12, 5898–5905.
Lee, U., Yoo, C.J., Kim, Y.J., Yoo, Y.M., 2016. Cytotoxicity of gold nanoparticles in human neural precursor cells and rat cerebral cortex. J. Biosci. Bioeng. 121, 341–344.
Li, Q., Barres, B.A., 2018. Microglia and macrophages in brain homeostasis and disease. Nat. Rev. Immunol. 18, 225.
Liddelow, S.A., Guttenplan, K.A., Clarke, L.E., Bennett, F.C., Bohlen, C.J., Schirmer, L., Bennett, M.L., Münch, A.E., Chung, W.-S., Peterson, T.C., 2017. Neurotoxic reactive astrocytes are induced by activated microglia. Nature 541, 481.
Liu, Y., Xu, Z., Li, X., 2013a. Cytotoxicity of titanium dioxide nanoparticles in rat neuroglia cells. Brain Inj. 27, 934–939.
Liu, Z., Shen, Y., Wu, Y., Yang, Y., Wu, J., Zhou, P., Lu, x., Guo, Z., 2013b. An intrinsic therapy of gold nanoparticles in focal cerebral ischemia-reperfusion injury in rats. J. Biomed. Nanotechnol. 9, 1017–1028.
Liz-Marzán, L.M., 2004. Nanometals: formation and color. Mater. Today 7, 26–31.
Long, T.C., Saleh, N., Tilton, R.D., Lowry, G.V., Veronesi, B., 2006. Titanium dioxide (P25) produces reactive oxygen species in immortalized brain microglia (BV2): implications for nanoparticle neurotoxicity. Environ. Sci. Technol. 40, 4346–4352.

Luther, E.M., Koehler, Y., Diendorf, J., Epple, M., Dringen, R., 2011. Accumulation of silver nanoparticles by cultured primary brain astrocytes. Nanotechnology 22, 375101.
Luther, E.M., Schmidt, M.M., Diendorf, J., Epple, M., Dringen, R., 2012. Upregulation of metallothioneins after exposure of cultured primary astrocytes to silver nanoparticles. Neurochem. Res. 37, 1639–1648.
Luther, E.M., Petters, C., Bulcke, F., Kaltz, A., Thiel, K., Bickmeyer, U., Dringen, R., 2013. Endocytotic uptake of iron oxide nanoparticles by cultured brain microglial cells. Acta Biomater. 9, 8454–8465.
Madhusudanan, P., Reade, S., Shankarappa, S.A., 2017. Neuroglia as targets for drug delivery systems: a review. Nanomed. Nanotechnol. Biol. Med. 13, 667–679.
Miao, Z., Gao, Z., Chen, R., Yu, X., Su, Z., Wei, G., 2018. Surface-bioengineered gold nanoparticles for biomedical applications. Curr. Med. Chem. 25, 1920–1944.
Morioka, T., Baba, T., Black, K.L., Streit, W.J., 1992. Response of microglial cells to experimental rat glioma. Glia 6, 75–79.
Mosquera, J.S., García, I., Henriksen-Lacey, M., González-Rubio, G., Liz-Marzán, L.M., 2018. Reducing protein Corona formation and enhancing colloidal stability of gold nanoparticles by capping with silica monolayers. Chem. Mater. 31, 57–61.
Mytych, J., Lewinska, A., Zebrowski, J., Wnuk, M., 2015. Gold nanoparticles promote oxidant-mediated activation of NF-κB and 53BP1 recruitment-based adaptive response in human astrocytes. Biomed Res. Int. 2015.
Nimmerjahn, A., Kirchhoff, F., Helmchen, F., 2005. Resting microglial cells are highly dynamic surveillants of brain parenchyma in vivo. Science 308, 1314–1318.
Pan, Y., Neuss, S., Leifert, A., Fischler, M., Wen, f., Simon, U., Schmid, G., Brandau, W., Jahnen-Dechent, W., 2007. Size-dependent cytotoxicity of gold nanoparticles. Small 3, 1941–1949.
Pan, Y., Leifert, A., Ruau, D., Neuss, S., Bornemann, J., Schmid, G., Brandau, W., Simon, U., Jahnen-Dechent, W., 2009. Gold nanoparticles of diameter 1.4 nm trigger necrosis by oxidative stress and mitochondrial damage. Small 5, 2067–2076.
Paxinos, G., Franklin, K.B., 2004. The Mouse Brain in Stereotaxic Coordinates. Gulf Professional Publishing.
Pérez-Arizti, J.A., Ventura-Gallegos, J.L., Juárez, R.E.G., del Pilar Ramos-Godinez, M., Colín-Val, X., López-Marure, R., 2020. Titanium dioxide nanoparticles promote oxidative stress, autophagy and reduce NLRP3 in primary rat astrocytes. Chem. Biol. Interact., 108966.
Petters, C., Thiel, K., Dringen, R., 2016. Lysosomal iron liberation is responsible for the vulnerability of brain microglial cells to iron oxide nanoparticles: comparison with neurons and astrocytes. Nanotoxicology 10, 332–342.
Rizvi, S.M.D., Hussain, T., Ahmed, A.B.F., Alshammari, T.M., Moin, A., Ahmed, M.Q., Barreto, G.E., Kamal, M.A., Ashraf, G.M., 2018. Gold nanoparticles: a plausible tool to combat neurological bacterial infections in humans. Biomed. Pharmacother. 107, 7–18.
Shah, M., Badwaik, V.D., Dakshinamurthy, R., 2014. Biological applications of gold nanoparticles. J. Nanosci. Nanotechnol. 14, 344–362.
Sharma, A.K., Singh, V., Gera, R., Purohit, M.P., Ghosh, D., 2017. Zinc oxide nanoparticle induces microglial death by NADPH-oxidase-independent reactive oxygen species as well as energy depletion. Mol. Neurobiol. 54, 6273–6286.
Sofroniew, M.V., 2009. Molecular dissection of reactive astrogliosis and glial scar formation. Trends Neurosci. 32, 638–647.
Sofroniew, M.V., 2015. Astrogliosis. Cold Spring Harb. Perspect. Biol. 7, a020420.
Sofroniew, M.V., Vinters, H.V., 2010. Astrocytes: biology and pathology. Acta Neuropathol. 119, 7–35.
Song, W.-J., Jeong, M.-S., Choi, D.-M., Kim, K.-N., Wie, M.-B., 2019. Zinc oxide nanoparticles induce autophagy and apoptosis via oxidative injury and pro-inflammatory cytokines in primary astrocyte cultures. Nanomaterials 9, 1043.
Sperling, R.A., Parak, W.J., 2010. Surface modification, functionalization and bioconjugation of colloidal inorganic nanoparticles. Philos. Trans. A Math. Phys. Eng. Sci. 368, 1333–1383.
Stojiljković, A., Kuehni-Boghenbor, K., Gaschen, V., Schüpbach, G., Mevissen, M., Kinnear, C., Möller, A.-M., Stoffel, M.H., 2016. High-content analysis of factors affecting gold nanoparticle uptake by neuronal and microglial cells in culture. Nanoscale 8, 16650–16661.
Streit, W.J., Graeber, M.B., Kreutzberg, G.W., 1988. Functional plasticity of microglia: a review. Glia 1, 301–307.
Sun, C., Yin, N., Wen, R., Liu, W., Jia, Y., Hu, L., Zhou, Q., Jiang, G., 2016. Silver nanoparticles induced neurotoxicity through oxidative stress in rat cerebral astrocytes is distinct from the effects of silver ions. Neurotoxicology 52, 210–221.
Wang, J., Deng, X., Zhang, F., Chen, D., Ding, W., 2014. ZnO nanoparticle-induced oxidative stress triggers apoptosis by activating JNK signaling pathway in cultured primary astrocytes. Nanoscale Res. Lett. 9, 1–12.
Wilson, C.L., Natarajan, V., Hayward, S.L., Khalimonchuk, O., Kidambi, S., 2015. Mitochondrial dysfunction and loss of glutamate uptake in primary astrocytes exposed to titanium dioxide nanoparticles. Nanoscale 7, 18477–18488.
Xia, Q., Huang, J., Feng, Q., Chen, X., Liu, X., Li, X., Zhang, T., Xiao, S., Li, H., Zhong, Z., 2019. Size-and cell type-dependent cellular uptake, cytotoxicity and in vivo distribution of gold nanoparticles. Int. J. Nanomedicine 14, 6957–6970.
Xu, L., Shao, A., Zhao, Y., Wang, Z., Zhang, C., Sun, Y., Deng, J., Chou, L.L., 2015. Neurotoxicity of silver nanoparticles in rat brain after intragastric exposure. J. Nanosci. Nanotechnol. 15, 4215–4223.
Xue, Y., Wu, J., Sun, J., 2012. Four types of inorganic nanoparticles stimulate the inflammatory reaction in brain microglia and damage neurons in vitro. Toxicol. Lett. 214, 91–98.
Zamanian, J.L., Xu, L., Foo, L.C., Nouri, N., Zhou, L., Giffard, R.G., Barres, B.A., 2012. Genomic analysis of reactive astrogliosis. J. Neurosci. 32, 6391–6410.
Zhang, X.-D., Wu, D., Shen, X., Chen, J., Sun, Y.-M., Liu, P.-X., Liang, X.-J., 2012. Size-dependent radiosensitization of PEG-coated gold nanoparticles for cancer radiation therapy. Biomaterials 33, 6408–6419.